

Simulation of the mantle and crustal helium isotope signature in the Mediterranean Sea using a high-resolution regional circulation model

M Ayache, J-C Dutay, P Jean-Baptiste, and E Fourré

Laboratoire des Sciences du Climat et de l'Environnement (LSCE), IPSL, CEA/UVSQ/CNRS, Orme des Merisiers, Gif-Sur-Yvette, France.

Correspondence to: M Ayache (mohamed.ayache@lsce.ipsl.fr)

Abstract.

Helium isotopes (^3He , ^4He) are useful tracers for investigating the deep ocean circulation and for evaluating ocean general circulation models, because helium is a stable and conservative nuclide that does not take part in any chemical or biological process. Helium in the ocean originates from three different sources: namely, (i) gas dissolution in equilibrium with atmospheric helium, (ii) helium-3 addition by radioactive decay of tritium (called tritiogenic helium), and (iii) injection of terrigenous helium-3 and helium-4 by the submarine volcanic activity which occurs mainly at plate boundaries, and also addition of (mainly) helium-4 from the crust and sedimentary cover by α -decay of uranium and thorium contained in various minerals.

We present the first simulation of the terrigenous helium isotope distribution in the whole Mediterranean Sea, using a high-resolution model (NEMO-MED12). For this simulation we build a simple source function for terrigenous helium isotopes based on published estimates of terrestrial helium fluxes. We estimate a hydrothermal flux of $3.5 \text{ mol } ^3\text{He yr}^{-1}$ and a lower limit for the crustal flux at $1.6 \times 10^{-7} \text{ mol } ^4\text{He mol m}^{-2} \text{ yr}^{-1}$.

24 In addition to providing constraints on helium isotope degassing fluxes in the
25 Mediterranean, our simulations provide information on the ventilation of the deep
26 Mediterranean waters which are useful for assessing NEMO-MED12 performance. This study is
27 part of the work carried out to assess the robustness of the NEMO-MED12 model, which will be
28 used to study the evolution the biogeochemical cycles in the Mediterranean Sea under a
29 changing climate, and to improve our ability to predict the future evolution of the Mediterranean
30 Sea under the increasing anthropogenic pressure.

31

32

33 **1 Introduction**

34 Helium isotopes are a powerful tool in Earth sciences. The ratio of ^3He to ^4He varies by more
35 than three orders of magnitude in terrestrial samples. This results from the distinct origins of
36 ^3He (essentially primordial) and ^4He (produced by the radioactive decay of uranium and thorium
37 series) and their contrasting proportions in the Earth's reservoirs (Fig.1). The atmospheric
38 ratio, $R_{\text{air}} = ^3\text{He}/^4\text{He} = 1.384 \times 10^{-6}$ (Clarke et al., 1976), can be considered constant due to
39 the long residence time of helium, which is $\sim 10^6$ times longer than the mixing time of the
40 atmosphere (based on the total helium content of the atmosphere and the global helium
41 degassing flux estimated by Torgersen, 1989). Relative to this atmospheric ratio, typical
42 $^3\text{He}/^4\text{He}$ ratios vary from $<0.1 R_{\text{air}}$ in the Earth's crust to an average of $8 \pm 1 R_{\text{air}}$ in the
43 upper mantle, and up to some 40 to 50 R_{air} in products of plume-related ocean islands, such
44 as Hawaii and Iceland (Ballentine and Burnard, 2002; Graham, 2002; Hilton et al., 2000).

45 At the ocean surface, helium is essentially in solubility equilibrium with the atmosphere.
46 However at depth, several important processes alter the isotopic ratio (Fig.1 - see Schlosser and
47 Winckler (2002) for review). Firstly, ^3He is produced by the radioactive decay of tritium (Jenkins
48 and Clark, 1976); and secondly terrigenic helium is introduced not only by the release of helium
49 from submarine volcanic activity at mid-ocean ridges and volcanic centres, with elevated
50 $^3\text{He}/^4\text{He}$ ratios typical of their mantle source (Lupton et al., 1977a, b; Jenkins et al., 1978;
51 Lupton, 1979; Craig and Lupton, 1981; Jean-Baptiste et al., 1991a, 1992); but also by the
52 addition of helium with a low $^3\text{He}/^4\text{He}$ ratio from the crust and sedimentary cover, mostly due to
53 α -decay of uranium and thorium minerals (Craig and Weiss, 1971).

54 Oceanic $^3\text{He}/^4\text{He}$ variations are usually expressed as $\delta^3\text{He}$, the percentage deviation from the
55 atmospheric ratio, defined as $(R_{\text{sample}}/R_{\text{air}} - 1)100$. Below the mixed layer, oceanic
56 $^3\text{He}/^4\text{He}$ values are usually significantly higher than the atmospheric ratio, with $\delta^3\text{He}$ up to
57 40% in the Pacific Ocean (Craig and Lupton, 1981; Lupton, 1998). However, there are some
58 exceptions. Intra-continental seas such as the Black Sea and the Mediterranean display deep
59 water $^3\text{He}/^4\text{He}$ ratios indicative of a preferential addition of ^4He -rich crustal helium rather than
60 ^3He -rich mantle helium (Top and Clarke, 1983; Top et al., 1991; Roether et al., 1998, 2013).

61 Early investigations in the eastern Mediterranean (Meteor cruise M5/1987, Roether et al.
62 (2013)) have indeed revealed that deep waters have a crustal helium signature, with $\delta^3\text{He}$ as low
63 as -5% (Fig. 2). Note that Fig. 2 shows this deep core of crustal helium **is** being progressively
64 erased by the addition of tritiogenic ^3He produced by the bomb tritium transient **and by the**
65 **recent dramatic changes in the thermohaline circulation of the EMed, known as the Eastern**
66 **Mediterranean Transient (EMT) (Roether et al., 1996, 2007, 2014), during which dense waters**
67 **of Aegean origin replaced the Adriatic source of the deep waters in the EMed.**

68 Deconvolution of the various helium components using neon indicates that the mantle helium
69 contribution is only ~5% (Roether et al., 1998). In the Mediterranean Sea terrigenous helium is
70 therefore largely of crustal origin due to the presence of a continental-type crust and a high
71 sediment load of continental origin, but also because mantle helium, which is produced by the
72 submarine volcanic activity in only a few places in the Mediterranean Sea (Eolian Arc, Aegean
73 Arc, Pantelleria Rift in particular), is released at rather shallow depths (Dando et al., 1999) and is
74 therefore quickly transferred to the atmosphere.

75 Mantle ³He was discovered in the deep ocean by Clarke et al., 1970. It is injected at mid-ocean
76 ridges as part of the processes generating new oceanic crust, and advected by ocean currents.
77 [Since this discovery](#), helium isotopes have been used extensively to trace the deep ocean
78 circulation (Jamous et al., 1992; Jean-Baptiste et al., 1991b, 1997, 2004; Lupton, 1996, 1998;
79 Top et al., 1991; R uth et al., 2000; Well et al., 2001; Srinivasan et al., 2004) and to study ocean
80 dynamics (circulation, ventilation and mixing processes) in conjunction with tritium (Andrie and
81 Merlivat, 1988; Jenkins, 1977, 1988; Schlosser et al., 1991; Roether et al., 2013). [Ventilation is](#)
82 [defined as the process of moving a parcel of water from the surface to a given subsurface](#)
83 [location. It can occur through convection, sub-duction, advection, and diffusion \(Goodman,](#)
84 [1997; England, 1995\).](#)

85 The helium isotope distribution in the deep oceans has also been simulated by various
86 ocean circulation models to constrain global helium degassing fluxes and evaluate the degree to
87 which models can correctly reproduce the main features of the world's ocean circulation
88 (Farley et al., 1995; Dutay et al., 2002, 2010; Bianchi et al., 2010).

89 In this study we build a source function for the release of terrigenous helium components (crust
90 and mantle) to the deep Mediterranean and apply it to a high-resolution oceanic model of the
91 Mediterranean Sea. The simulated helium-isotope distribution is then compared with available
92 data (see §4) to constrain terrigenous helium fluxes. In addition to providing constraints on the
93 degassing flux, our work is the first attempt to simulate natural helium-3 in a high-resolution
94 regional model of the Mediterranean Sea and provides new information on the model's capacity
95 to represent the ventilation of deep waters.

96

97

98 2 Description of the model

99 The model used in this work is a free surface ocean general circulation model NEMO
100 (Nucleus for European Modelling of the Ocean) (Madec and NEMO-Team., 2008) in a regional
101 configuration called NEMO-MED12 (Beuvier et al., 2012a).

102 This model of the Mediterranean Sea has been used previously to study anthropogenic tritium
103 and its decay product helium-3 (Ayache et al., 2015), the anthropogenic carbon uptake (Palmiéri
104 et al., 2015), the transport through the Strait of Gibraltar (Soto-Navarro et al., 2014), as well as
105 the Western Mediterranean Deep Water (WMDW) formation (Beuvier et al., 2012a), and the
106 mixed layer response under high-resolution air-sea forcings (Lebeaupin Brossier et al., 2011).
107 This model satisfactorily simulates the main structures of the thermohaline circulation of the
108 Mediterranean Sea, with mechanisms having a realistic timescale compared to observations. In
109 particular, tritium/helium-3 simulations (Ayache et al., 2015) have shown that the Eastern
110 Mediterranean Transient (EMT) signal from the Aegean sub-basin is realistically simulated,
111 with its corresponding penetration of tracers into the deep water in early 1995. The strong
112 convection event of winter 2005 and the following years in the Gulf of Lions was satisfactorily
113 captured as well. However, some aspects of the model still need to be improved: in the eastern
114 basin, tritium/helium-3 simulations have highlighted the too- weak formation of Adriatic Deep
115 Water (AdDW), followed by a weak contribution to the EMDW in the Ionian sub-basin. In the
116 western basin, the production of WMDW is correct, but the spreading of the recently ventilated
117 deep water to the south of the basin is too weak. The consequences of these weaknesses in the
118 model's skill at simulating some important aspects of the dynamics of the deep ventilation of
119 the Mediterranean will have to be kept in mind when analysing these helium simulations.

120 NEMO-MED12 covers the whole Mediterranean Sea, but also extends into the Atlantic
121 Ocean. Horizontal resolution is one-twelfth of a degree, thus varying with latitude between 8
122 and 6.5 and 8 km from 30° N to 46° N, respectively, and between 5.5 and 7.5 km in longitude.
123 Vertical resolution varies with depth, from 1 m at the surface, to 450 m at the bottom (50 levels
124 in total). We use partial-steps to adjust the last numerical level with the bathymetry. [The](#)
125 [exchanges with the Atlantic Ocean are performed through a buffer zone, from 11°W to 7.5°](#),
126 where 3-D temperature and salinity model fields are relaxed to the observed climatology
127 (Beuvier et al., 2012a). NEMO-MED12 is forced at the surface by ARPERA (Herrmann and
128 Somot, 2008; Herrmann et al., 2010) daily fields of the momentum, evaporation and heat fluxes
129 over the period 1958-2013. For the sea-surface temperature (SST) a relaxation term is applied to
130 the heat flux (Beuvier et al., 2012a). The total volume of water in the Mediterranean Sea is
131 conserved by restoring the sea-surface height (SSH) in the Atlantic buffer zone toward the
132 GLORYS1 reanalysis (Ferry et al., 2010).

133 The initial conditions (temperature, salinity) for the Mediterranean Sea are prescribed from the
134 MedAtlas-II (MEDAR-MedAtlas-group, 2002; Rixen et al., 2005) climatology weighted by a
135 low-pass filter with a time window of 10 years using the MedAtlas data covering the 1955-1965
136 period, following Beuvier et al. (2012a). For the Atlantic buffer zone, the initial state is set from
137 the 2005 World Ocean Atlas for temperature (Locarnini et al., 2006), and salinity (Antonov et
138 al., 2006). River runoff is prescribed from the interannual data set of Ludwig et al. (2009) and
139 Vörösmarty et al. (1996).

140 Full details of the model and its parameterizations are described by Beuvier et al. (2012a, b);
141 Palmiéri et al. (2015) and (Ayache et al., 2015).

142

143 **3 The tracer model**

144 Helium is implemented in the model as a passive conservative tracer which does not affect
145 ocean circulation. It is transported in the Mediterranean Sea by NEMO-MED12 physical fields
146 using an advection-diffusion equation (Eq. 1). The rate of change of the concentration of each
147 specific passive tracer C is:

148
$$\frac{\partial C}{\partial t} = S(C) - U \cdot \nabla C + \nabla \cdot (K \nabla C) \quad (1)$$

149 where $S(C)$ is the tracer source (at the seafloor) and sink (at the air-sea interface); $U \cdot \nabla C$ is
150 advection of the tracer along the three perpendicular axes and $\nabla \cdot (K \nabla C)$ is the lateral and
151 vertical diffusion, with the same parameterization as for the hydrographic tracers.

152 Because ^3He , ^4He are passive tracers, simulations could be run in a computationally efficient
153 off-line mode. This method relies on previously computed circulation fields (U , V , W) from the
154 NEMO-MED12 dynamical model (Beuvier et al., 2012a). Physical forcing fields are read daily
155 and interpolated to give values for each 20-min time-step. The same approach was used by
156 Ayache et al. (2015) to model the anthropogenic tritium invasion and by Palmiéri et al. (2015)
157 for simulating CFCs and anthropogenic carbon. This choice is justified by the fact that these
158 tracers are passive. Their injection does not alter the dynamics of the ocean, and they have no
159 influence on the physical properties of water, unlike hydrographic tracers such as temperature or
160 salinity.

161 The simulations were initialized with uniform ^3He and ^4He concentrations corresponding to
162 those at solubility equilibrium with the partial pressures of these isotopes in the atmosphere, for
163 seawater at $T=10^\circ\text{C}$ and $S=34$ (Weiss, 1971). Model simulations were integrated for five

164 hundred years until they reached a quasi-steady state, i.e., the globally averaged drift was less
165 than $10^{-2} \delta^3\text{He}$ % per two hundred years of run

166 **3.1 Parameterization of the helium injection**

167 Terrigenous helium in the Mediterranean Sea has two components: 1) Crustal helium, originating
168 from the crust and overlying sediment cover, and 2) mantle helium, injected by submarine
169 volcanic activity. For the injection of helium, we follow the protocol proposed by (Dutay et al.,
170 2002, 2004), and (Farley et al., 1995). Each component has a characteristic $^3\text{He}/^4\text{He}$ value. The
171 anthropogenic ^3He distribution due to the decay of bomb tritium has already been addressed
172 by Ayache et al., 2015.

173 For this study, we ran two separate simulations, one for each helium component. Each
174 simulation has two boundary conditions: a loss term at the surface, due to the sea-to-air gas
175 exchange, and a source term at the seafloor, describing terrigenous tracer input. Each simulation
176 thus represents the sum of the specified terrigenous component and the atmospheric component,
177 with the distributions of ^3He and ^4He computed separately. We then calculate the isotopic ratio
178 using the $\delta^3\text{He}$ notation.

179

180 **3.1.1 Surface boundary condition**

181 The only sink for oceanic helium is loss to the atmosphere. At the air-sea interface, the model
182 will exchange ^3He and ^4He with the atmosphere using sea-air flux boundary conditions that are
183 analogous to those developed for helium during the second phase of OCMIP
184 <http://ocmip5.ipsl.jussieu.fr/OCMIP/phase2/simulations/Helium/HOWTO-Helium.html> (Dutay
185 et al., 2002). Using the standard flux-gradient formulation for a passive gaseous tracer, the flux
186 of helium, F_{He} is given by:

187 $F_{\text{He}} = K_w(C_{\text{eq}} - C_{\text{surf}})$ (2)

188 where K_w is the gas transfer (piston) velocity [m s^{-1}], C_{surf} is the modelled surface ocean
189 concentration of ^3He or ^4He as appropriate, and C_{eq} is the atmospheric solubility equilibrium
190 concentration (Weiss, 1971) at the local sea-surface temperature (SST) and salinity (SSS).

191 Here, we neglect spatio-temporal variations in atmospheric pressure and assume it remains at 1
192 atm. The gas transfer velocity is computed from surface-level wind speeds, u , [m s^{-1}] from the
193 ARPERA forcing (Herrmann and Somot, 2008; Herrmann et al., 2010) following the
194 Wanninkhof (1992, Eq. 4) formulation:

195 $K_w = a u^2 (\text{Sc} / 660)^{-1/2}$ (3)

196 where $a = 0.31$ and Sc is the Schmidt number which is to be computed from the modelled SST,
197 using the formulation for ^4He given by Wanninkhof (1992), derived from Jähne et al. (1987a).
198 For ^3He , we reduce the Schmidt number (relative to ^4He) by 15% ($\text{ScHe-3} = \text{ScHe-4} / 1.15$)
199 based on the ratio of the reduced masses, which is consistent with helium isotopic fractionation
200 measurements by Jähne et al. (1987b). **Therefore, in the following, the modelled atmospheric**
201 **component is the helium distribution at equilibrium with surface air-sea boundary conditions,**
202 **without any helium flux from the seafloor.**

203 **3.1.2 Crustal helium fluxes**

204 Lake and groundwater studies have shown that radiogenic helium is continuously released from
205 the underlying crustal bedrock (see Kipfer et al., 2002 for review). Porewaters trapped in
206 oceanic sediments are also enriched in radiogenic ^4He from the underlying oceanic crust and in
207 situ ^4He production by uranium- and thorium-rich minerals, releasing their helium at the sea
208 bottom (Wakita et al., 1985; Sano and Wakita, 1985; Sano et al., 1987; Chaduteau et al., 2009).
209 Deep waters of intra-continental seas such as the Mediterranean are more prone to exhibit a
210 radiogenic ^4He signature than the open ocean because the continental upper crust is about 40

211 times more enriched in uranium and thorium than the oceanic crust (Taylor and McLennan,
212 1985; Torgersen, 1989). In the deep eastern Mediterranean, southwest of Crete, extremely high
213 radiogenic ^4He concentrations have indeed been measured in deep brine pools created by the
214 advection of deep buried fluids hosted by the sedimentary matrix beneath the Messinian
215 evaporites (Winckler et al. 1997; Charlou et al., 2003). However, there are no data on the spatial
216 variability of the crustal helium injection to deep waters. Therefore in the model, crustal helium
217 is injected as a uniform flux (in mol of helium per square metre of seafloor > 1000 m) with a
218 $^3\text{He}/^4\text{He}$ ratio of $0.06 R_{\text{air}}$ (Winckler et al. 1997; Charlou et al., 2003). The initial value of this
219 flux is that estimated by Roether et al. (1998) (Table 2) using a multi-box model in which the
220 thermohaline circulation of the eastern Mediterranean is represented by a deep-water reservoir
221 (> 1000 m depth) and two intermediate water cells (Roether et al., 1994) (see Table 2).
222 Sensitivity tests were made to determine the flux which produces the best agreement with
223 available data (Roether et al., 1998; Roether et al., 2013).

224 **3.1.3 Mantle helium fluxes**

225 The subduction of the African plate below Europe is responsible for the volcanic activity which
226 takes place in the Mediterranean basin (Fig. 3). The main submarine activity is found in the
227 Tyrrhenian and Aegean Seas, and in the Sicily Channel (Dando et al., 1999).

228 Hydrothermal vents in the Tyrrhenian sub-basin are found all along the Eolian volcanic Arc
229 (Fig. 3) from Palinuro in the north to Eolo and Enarete in the southwest (Lupton et al., 2011), as
230 well as on the Marsili seamount (Lupton et al., 2011).

231 In the Aegean, hydrothermal systems occur along the southern Aegean Volcanic Arc from
232 Sousaka and Methana in the west to Kos, Yali and Nisiros in the east (Dando et al., 1999).

233 Finally, a recent helium isotope survey across the Sicily Channel, which separates the Sicilian
234 platform from Africa, also suggests hydrothermal helium input between 600 and 700 m depth
235 associated with the Pantelleria rift (Fourré and Jean-Baptiste, unpublished results).
236 Location and depth of the active zones are shown in Fig. 3. Table 1 summarizes the ^3He fluxes
237 used for our simulations. For the Eolian and Aegean volcanic arc, ^3He fluxes were determined
238 by simple scaling to the global ^3He flux from arc volcanism, which can be estimated (to within a
239 factor of two) to be $\sim 4 \times 10^{-3}$ ^3He mol per km of arc based on the assumption that the magma
240 production rate of arcs is $\sim 20\%$ of that of Mid-Ocean-Ridges (Torgersen, 1989; Hilton et al.,
241 2002) and the total length of subduction zones. For the Marsili seamount, the ^3He flux was
242 estimated from ^3He fluxes at nearby subaerial volcanoes (Allard, 1992a, 1992b). $^3\text{He}/^4\text{He}$
243 isotopic ratios were chosen according to available in situ data (when available) or to $^3\text{He}/^4\text{He}$
244 data from nearby subaerial volcanoes.

245

246 **4. Observations used for the comparison with model results**

247 The tracer data in the Mediterranean which are relevant for comparison with model results are
248 the Meteor cruises across the Eastern Mediterranean basin (Roether et al., 2013 - see Fig. 2) and
249 the helium isotope survey carried out by Lupton et al., 2011 in the Tyrrhenian sea. Additional
250 $\delta^3\text{He}$ data (Fourré and Jean-Baptiste, unpublished data) from the Nov. 2013 Record cruise in the
251 Sicily channel (Geotraces program) are also available. 1987 Meteor section is of particular
252 interest since it is the less affected by tritiogenic ^3He (Fig. 2) and therefore the deconvolution of
253 the various helium components using neon is the most accurate. This deconvolution is carried
254 out using the method proposed by Roether et al., 1998; 2001, which allows to derive the
255 atmospheric helium component from the neon distribution and then to obtain the terrigenic

256 helium-4 component by subtracting this atmospheric component from the total measured
257 helium concentration. The atmospheric and terrigenous helium-3 components are then obtained
258 using the $^3\text{He}/^4\text{He}$ ratios of dissolved atmospheric and terrigenous helium, respectively. For the
259 Tyrrhenian sea, the $\delta^3\text{He}$ excess due to hydrothermal activity along the Aeolian arc is obtained
260 by subtracting the background vertical $\delta^3\text{He}$ profile of vertical cast V01 (see Lupton et al.,
261 2011) to the measured $\delta^3\text{He}$. The same method was used for Sicily channel data. Accuracy of
262 the deconvoluted $\delta^3\text{He}$ is in the range 1%-1.5%.

263

264 **5. Results**

265 **5.1 Crustal helium distribution**

266 We begin our analysis by providing an overview of the simulated crustal+atmospheric helium
267 component. Figure 4a displays a section of modelled $\delta^3\text{He}_{\text{crust+atm}}$ along a W-E transect across
268 the eastern basin (EMed). As expected, the $\delta^3\text{He}_{\text{crust+atm}}$ distribution exhibits negative values,
269 predominately in the deep waters, hinting at the presence of crustal-He highly enriched in
270 radiogenic ^4He . The model correctly simulates the crustal-He distribution in the Levantine sub-
271 basin (Fig. 4c), where the simulated $\delta^3\text{He}_{\text{crust+atm}}$ values agrees reasonably well with observations
272 from Meteor cruise M5. However, modelled $\delta^3\text{He}_{\text{crust+atm}}$ values for the deep Ionian sub-basin
273 are too low, with a mean value below 3500 m around -7 % compared to $-4.5\pm 0.7\%$ in the data
274 (Fig. 4d). This too-large an accumulation of crustal ^4He is the expected consequence of the too-
275 low ventilation of the deep Ionian sub-basin in the model, as already diagnosed in the
276 anthropogenic tritium- ^3He simulations of Ayache et al. (2015). The model generates a too-weak
277 formation of Adriatic Deep Waters (AdDW) that prevents the model from reproducing the
278 observed signal associated with injection at depth of surface water.

279 The simulated $\delta^3\text{He}_{\text{crust+atm}}$ distribution in the western basin (Fig. 4b) shows the same gradient as
280 in the Levantine basin with negative values in the deep water (values around -5.5%), as a result
281 of the homogenous crustal-He flux over the whole basin (see Sect. 3). In the surface layer
282 helium in solution is essentially in equilibrium with atmospheric helium ($\delta^3\text{He}_{\text{crust+atm}}$ values
283 around -1.6%), but decreasing steadily with depth down to a layer of minimum $\delta^3\text{He}_{\text{crust+atm}}$
284 values in deep waters. Although the terrigenic component cannot be estimated quantitatively
285 for the WMed because of the lack of a precise value for its $3\text{He}/4\text{He}$ ratio (R_{ter}), the lower limit
286 of $\delta^3\text{He}_{\text{crust+atm}}$ (taking R_{ter} equal to zero) is in the range -3.5% - -4.5% for deep waters. This is
287 less radiogenic than in the Eastern basin, in agreement with the conclusions of Rhein et al.
288 (1999) that the crustal component may be small in the WMed. Our model results (-5.5% on
289 average) is somewhat lower, suggesting that, as already observed in the Eastern basin, the model
290 probably underestimates the ventilation rate of deep waters in the western basin too.

291

292 **5.2 Mantle helium distribution**

293 As discussed above, the main active submarine volcanic systems are located in the Tyrrhenian,
294 Aegean Seas and the Sicily Channel (Fig. 3).

295 **5.2.1 Pantelleria Rift**

296 In the Pantelleria Rift, a clearly visible plume of mantle helium is simulated between 500 and
297 1000 m depth (Fig. 5a). The modelled $\delta^3\text{He}$ plume anomaly at 12°E reaches a maximum value
298 of 2.5% above the atmospheric background of -1.6% . This value is in good agreement with in
299 situ observations at the same location (2.3% above background at 800 m, Fig. 5d; Fourré and
300 Jean-Baptiste, unpublished data).

301 **5.2.2 Tyrrhenian Sea**

302 The submarine volcanic activity in the Tyrrhenian is essentially confined to depths below 1200
303 m. The corresponding mantle helium input creates a weak but well-defined $\delta^3\text{He}$ plume (Fig.
304 5b) centred around 1000 m depth, which propagates into the entire Tyrrhenian sub-basin (Fig.
305 6). Average simulated $\delta^3\text{He}$ values above the atmospheric background (-1.6%) are within $\delta^3\text{He}$
306 = - 0.5% of the corresponding above-background $\delta^3\text{He}$ measurements of Lupton et al. (2011) in
307 the same area (Figs. 5b and 5e).

308 **5.2.3 Aegean Sea**

309 Hydrothermal venting in the Aegean sub-basin occurs at shallow depths (between 50 and 450 m
310 depth) compared to the two other sites in the Mediterranean Sea; in consequence the simulated
311 $\delta^3\text{He}_{\text{mantle+atm}}$ anomaly is particularly weak in this area due to the rapid helium degassing into the
312 atmosphere (Fig. 5c) and the signal does not propagate into the larger area around the Aegean
313 sea (Fig. 6). Note that no $\delta^3\text{He}$ data are available for comparison in the Aegean basin.

314 Figure 6 provides a descriptive view of the global distribution of the modelled $\delta^3\text{He}_{\text{mantle+atm}}$
315 signal over the Mediterranean Sea. The figure highlights the location of mantle-He sources, and
316 of their propagation through the interior of the Mediterranean Sea. The $\delta^3\text{He}_{\text{mantle+atm}}$ anomaly is
317 clearly visible over the three main areas of submarine volcanic activity. The mantle-He plume
318 injected by the Aeolian Arc spreads over the entire Tyrrhenian sub-basin, then leaves through
319 the Corsican Channel (1900 m), and extends into the Liguro-Provençal sub-basin associated
320 with the [Levantine Intermediate Water \(LIW\)](#) trajectory, and in the Algerian sub-basin through
321 the Sardinian Channel. The input from the Pantelleria Rift is topographically trapped in the
322 Sicilian channel. The Aegean sub-basin is also impacted by the mantle-He: the He excess is
323 localised in the western part of this sub-basin between mainland Greece and the island of Crete.

324

325 **5.3 Total helium-3 distribution**

326 The Mediterranean Sea is characterized by coexisting terrigenous and tritiogenic helium
327 throughout its subsurface waters. Fig. 7 presents a model-data comparison of the simulated total
328 $\delta^3\text{He}$ (sum of terrigenous, tritiogenic and atmospheric helium) in 1987, along the W-E Emed
329 transect corresponding to Meteor 5 cruise (1987). The tritiogenic component in 1987 is taken
330 from Ayache et al. (2015). Figure 7, exhibits a $\delta^3\text{He}$ maximum at a few hundred metres depth,
331 hinting at the presence of tritiogenic ^3He produced by the radioactive decay of anthropogenic
332 bomb-tritium. Further down $\delta^3\text{He}$ values decrease, and in the Levantine basin, even dropping
333 below the value for solubility equilibrium with the atmosphere ($\sim -1.6\%$). This represents the
334 signature of crustal helium in the deep Mediterranean waters.

335 The model correctly reproduces the $\delta^3\text{He}$ maximum of the intermediate waters, with values
336 similar to observations, except in the eastern part of the section where it tends to be
337 overestimated. Deeper, we have a realistic simulation of the helium signal in the Levantine sub-
338 basin (Fig. 7b) with $\delta^3\text{He}$ around -5% , which is in good agreement with observations made
339 during Meteor cruise M5, with only 10% of difference between the simulated $\delta^3\text{He}$ mean
340 vertical profile and in-situ data below 2000 m depth (Fig. 7b). Again one can clearly see the
341 shortcoming associated with the too-weak EMDW formation in the Adriatic sub-basin, leads to
342 too-negative $\delta^3\text{He}$ values at depth: the model tends to underestimate the $\delta^3\text{He}$ levels in the deep
343 water by more than 60 % compared to observations below 2000 m depth (Fig.7c).

344 Comparison of the tritiogenic and mantle $\delta^3\text{He}$ signatures, which occur at similar depths in the
345 Mediterranean Sea, shows that tritiogenic ^3He clearly dominates over mantle ^3He . This finding
346 agrees with those of Roether and Lupton (2011) for the Tyrrhenean basin; they concluded that
347 most of the helium-3 excess is tritiogenic.

6. Discussion

We have presented the first simulation of the terrigenous helium isotope distribution in the Mediterranean Sea, using a high-resolution model (NEMO-MED12). For this simulation we built a source function for terrigenous (crustal and mantle) helium isotopes obtained by simple scaling of published flux estimates (Table 1 and 2). For crustal helium, our helium flux equal to $1.6 \cdot 10^{-7} \text{ mol } ^4\text{He m}^{-2} \text{ yr}^{-1}$, generates a satisfying agreement with the data in the Levantine basin, where the tritium/ ^3He simulations of Ayache et al. (2015) have shown that modelled ventilation of the deep waters is correct. This flux represents only 10% of the previous estimate by Roether et al. (1998) for the eastern Mediterranean ($1.6 \cdot 10^{-6} \text{ mol m}^{-2} \text{ yr}^{-1}$), based on a box-model where the thermohaline circulation of the eastern Mediterranean is represented by a deep-water reservoir (> 1000 m depth) and two intermediate water cells. ~~The Roether et al. (1998) estimate falls in the range of the helium continental flux, 1.4 to 2.2 $\cdot 10^{-6} \text{ mol m}^{-2} \text{ yr}^{-1}$ (see Table 2). However, Winekler et al. (1997) have shown that the thick evaporites layer deposited during the Messinian Salinity Crisis in the Mediterranean Sea acts as a barrier to the upward diffusion of helium from deeper strata. Hence, the expected crustal helium flux from the Mediterranean seafloor may be reduced compared to the “pure” continental value, so the Roether et al. model estimate may be too high.~~

The tritium/ ^3He (Ayache et al., 2015) and CFC (Palmiéri et al., 2015) simulations have shown that the model adequately represents ventilation of near-surface and intermediate waters but globally underestimates the ventilation rate of the Mediterranean deep waters, particularly in the Ionian sub-basin, where the deep-water ventilation associated with the Adriatic Deep Water (AdDW) is too shallow in the simulations compared to observations. This mismatch is likely due to an overestimation of the freshwater flux (Precipitation-Evaporation and runoff) into the

371 Adriatic sub-basin. Taking into account this model deficiency, our estimate must definitely be
372 considered as a lower limit of the crustal helium flux into the Mediterranean basin.

373 For mantle helium, our simple parameterization produces realistic simulated $\delta^3\text{He}$ values that
374 are in agreement with in situ measurements, thus supporting our scaling approach. This study
375 provides a useful constraint on the magnitude of the hydrothermal helium-3 fluxes in the
376 Mediterranean Sea (Table 1), that is of interest because this flux can be now used to estimate the
377 hydrothermal flux of other chemical species. Hydrothermal venting produces plumes in the
378 ocean that are highly enriched in a variety of chemical species. Hydrothermal activity impacts
379 the global cycling of elements in the ocean (Elderfield and Schultz, 1996), including
380 economically valuable minerals, such as rare-earth elements (REE) which are deposited in deep
381 sea sediments. These minerals are crucial in the manufacture of novel electronic equipment and
382 green-energy technologies (Kato et al., 2011). Hydrothermal chemical elements such as iron
383 also impact biological cycles and eventually the carbon cycle and climate (Tagliabue et al.,
384 2010). Our simulations show that high-resolution oceanic models coupled with measurements of
385 conservative hydrothermal tracers such as helium isotopes can be useful tools to study the
386 environmental impact of hydrothermal activity in a variety of marine environments and at a
387 variety of scales. Beyond the case of hydrothermal activity, it also shows that high-resolution
388 ocean circulation models such as NEMO-MED 12 are well suited to the study of the evolution
389 of quasi-enclosed basins such as the Mediterranean Sea that are under increasing anthropogenic
390 pressure.

391 The global inventory of helium isotopes in the Mediterranean Sea based on our simulations
392 indicates the relative contribution of each source of the tracer (Table 3). Besides atmospheric
393 helium, which is the main source for both ^3He and ^4He , it shows that tritiogenic ^3He and crustal
394 ^4He are the main contributors to ^3He and ^4He excesses over solubility equilibrium. Therefore, in

395 contrast with the world's oceans where mantle helium dominates over other terrigenous and
396 tritiogenic components, the mantle helium component linked to the submarine
397 volcanic/hydrothermal activity is relatively small compared to the other sources of helium in the
398 Mediterranean Sea. This is due to the cumulated effects of (1) the relatively shallow depths of
399 hydrothermal injections in the Mediterranean (<1000 m) compared to the Mid-Ocean Ridges
400 (MOR), mostly in the range 2000 - 4000 m that favour a more rapid degassing through the air-
401 sea interface; (2) lower helium flux from arc volcanism (20%) compared to MOR volcanism
402 (Torgersen, 1989; Hilton et al, 2002); and (3) high crustal-He flux in the Mediterranean basin
403 due to its intra-continental nature (i.e., with a continental-type crust and high sediment load of
404 continental origin). However, despite its minor contribution to the global helium-3 budget, the
405 hydrothermal component remains identifiable due to its elevated isotopic signature.

406

407 **7 Conclusions**

408 The terrigenous helium isotope distribution was simulated for the first time in the whole
409 Mediterranean Sea, using a high-resolution model (NEMO-MED12) at one-twelfth of a degree
410 horizontal resolution (6–8 km). The parameterization of the helium injection at the seafloor led
411 to results of sufficient quality to allow us to put valuable constraints on the crustal and mantle
412 helium fluxes. Helium simulations also confirmed some shortcomings of the model dynamics in
413 representing the deep ventilation of the Ionian basin, already pinpointed by recent transient
414 tracer studies. [In spite of these limitations and of the limited data set at our disposal for model-
415 data comparison](#), our work puts additional constraints on the origin of the helium isotopic
416 signature in the Mediterranean Sea. The simulation of this tracer and its comparison with
417 observations provide a new and additional technique for assessing and improving the dynamical
418 regional model NEMO-MED12. This is essential if we are to improve our ability to predict the

419 future evolution of the Mediterranean Sea under the increasing anthropogenic pressure it is
420 suffering (Drobinski et al., 2012). It also offers new opportunities to study chemical element
421 cycling particularly in the context of the increasing amount of data that will result from the
422 international GEOTRACES effort (GEOTRACES, 2007).

423

424

425

426 **References**

427 The references will be generated automatically by Mendeley (in the latex version).

428 Allard, P.: Global emissions of helium-3 by subaerial volcanism, *Geophysical Research Letters*,
429 19, 1479–1481, doi:10.1029/92GL00974, <http://doi.wiley.com/10.1029/92GL00974>, 1992a.

430 Allard, P.: Correction to “Global emissions of helium-3 by subaerial volcanism”, *Geophysical*
431 *Research Letters*, 370 19, 2103–2103, doi:10.1029/92GL02477,
432 <http://doi.wiley.com/10.1029/92GL02477>, 1992b.

433 Andrie, C. and Merlivat, L.: Tritium in the western Mediterranean Sea during 1981 Phycemed
434 cruise, *Deep-Sea Research Part A. Oceanographic Research Papers*, 35, 247–267,
435 doi:10.1016/0198-0149(88)90039-
436 8, <http://www.sciencedirect.com/science/article/pii/0198014988900398>, 1988.

437 Antonov, J. I., Locarnini, R. A., Boyer, T. P., Mishonov, A. V., and Garcia, H. E.: *World Ocean*
438 *Atlas 2005*, 375 Volume 2: Salinity, S. Levitus, Ed, NOAA Atlas NESDIS 62, U.S.
439 Government Printing Office, Washington, D.C., p. 182 pp, 2006.

440 Ayache, M., Dutay, J.-C., Jean-Baptiste, P., Beranger, K., Arsouze, T., Beuvier, J., Palmieri, J.,
441 Le-vu, B., and Roether, W.: Modelling of the anthropogenic tritium transient and its decay
442 product helium-3 in the Mediterranean Sea using a high-resolution regional model, *Ocean*
443 *Science*, 11, 323–342, doi:10.5194/os-11-323-380 2015, [http://www.ocean-](http://www.ocean-sci.net/11/323/2015/os-11-323-2015.html)
444 [sci.net/11/323/2015/os-11-323-2015.html](http://www.ocean-sci.net/11/323/2015/os-11-323-2015.html), 2015.

445 Ballentine, C. J. and Burnard, P. G.: Production, Release and Transport of Noble Gases in the
446 Continental Crust, *Reviews in Mineralogy and Geochemistry*, 47, 481–538,
447 doi:10.2138/rmg.2002.47.12, <http://rimg.geoscienceworld.org/content/47/1/481> <http://rimg.g>

eoscienceworld.org/cgi/doi/10.2138/rmg.2002.47.12,2002.

- 448
449 Beuvier, J., Béranger, K., Lebeau-pin Brossier, C., Somot, S., Sevault, F., Drillet, Y., Bourdallé-
450 Badie, R., Ferry, N., and Lyard, F.: Spreading of the Western Mediterranean Deep Water
451 after winter 2005: time scales and deep cyclone transport, *Journal of Geophysical*
452 *Research*, 117, C07 022, doi:10.1029/2011JC007679,
453 <http://doi.wiley.com/10.1029/2011JC007679>, 2012a.
- 454 Beuvier, J., Lebeau-pin Brossier, C., Béranger, K., Arsouze, T., Bourdallé-Badie, R., Deltel, C.,
455 Drillet, Y., Drobinski, P., Lyard, F., Ferry, N., Sevault, F., , and Somot, S.:MED12,
456 Oceanic component for the modeling of the regional Mediterranean Earth System,
457 *Mercator Ocean Quarterly Newsletter*, 46, 60–66, 2012b.
- 458 Bianchi, D., Sarmiento, J. L., Gnanadesikan, A., Key, R. M., Schlosser, P., and Newton, R.:
459 Low helium flux from the mantle inferred from simulations of oceanic helium isotope data,
460 *Earth and Planetary Science Letters*, 297, 379–386, doi:10.1016/j.epsl.2010.06.037,
461 <http://www.sciencedirect.com/science/article/395 pii/S0012821X10004127>, 2010.
- 462 Capaccioni, B., Tassi, F., Vaselli, O., Tedesco, D., and Poreda, R.: Submarine gas burst at
463 Panarea Island (southern Italy) on 3 November 2002: A magmatic versus hydrothermal
464 episode, *Journal of Geophysical Research*, 112, B05 201, doi:10.1029/2006JB004359,
465 <http://doi.wiley.com/10.1029/2006JB004359>, 2007.
- 466 Capasso, G., Carapezza, M. L., Federico, C., Inguaggiato, S., and Rizzo, A.: Geochemical
467 monitoring of the 2002–2003 eruption at Stromboli volcano (Italy): precursory changes in
468 the carbon and helium isotopic composition of fumarole gases and thermal waters, *Bulletin*
469 *of Volcanology*, 68, 118–134, doi:10.1007/s00445-005-0427-5,
470 <http://link.springer.com/10.1007/s00445-005-0427-5>, 2005.
- 471 Chaduteau, C., Jean-Baptiste, P., Fourré, E., Charlou, J.-L., and Donval, J.-P.: Helium transport
472 in sediment pore fluids of the Congo-Angola margin, *Geochemistry, Geophysics,*
473 *Geosystems*, 10, n/a–n/a, 405 doi:10.1029/2007GC001897,
474 <http://doi.wiley.com/10.1029/2007GC001897>, 2009.
- 475 Charlou, J., Donval, J., Zitter, T., Roy, N., Jean-Baptiste, P., Foucher, J., and Woodside, J.:
476 Evidence of methane venting and geochemistry of brines on mud volcanoes of the eastern
477 Mediterranean Sea, *Deep Sea Research Part I: Oceanographic Research Papers*, 50, 941–
478 958, doi:10.1016/S0967-0637(03)00093-
479 1,<http://www.sciencedirect.com/science/article/pii/S0967063703000931>, 2003.
- 480 Clarke, W., Jenkins, W., and Top, Z.: Determination of tritium by mass spectrometric
481 measurement of ^3He , *The International Journal of Applied Radiation and Isotopes*, 27,
482 515–522, doi:10.1016/0020-708X(76)90082-X,
483 <http://www.sciencedirect.com/science/article/pii/0020708X7690082X>, 1976.

- 484 Clarke, W. B., Beg, M. A., and Craig, H.: Excess helium 3 at the North Pacific Geosecs Station,
485 *Journal of Geophysical Research*, 75, 7676–7678, doi:10.1029/JC075i036p07676,
486 <http://doi.wiley.com/10.1029/JC075i036p07676>, 1970.
- 487 Craig, H. and Lupton, J. E.: Helium-3 and mantle volatiles in the ocean and the oceanic crust,
488 *Oceanic Lithosphere*, 7, 391–428, 1981.
- 489 Craig, H. and Weiss, R. F.: Dissolved gas saturation anomalies and excess helium in the ocean,
490 *Earth and Planetary Science Letters*, 10 (3), 289–296, 1971.
- 491 D’Alessandro, W., De Gregorio, S., Dongarrà, G., Gurrieri, S., Parello, F., and Parisi, B.:
492 Chemical and isotopic characterization of the gases of Mount Etna (Italy), *Journal of*
493 *Volcanology and Geothermal Research*, 78, 65–76, doi:10.1016/S0377-0273(97)00003-6,
494 <http://www.sciencedirect.com/science/article/pii/S0377027397000036>, 1997.
- 495 Dando, P., Stüben, D., and Varnavas, S.: Hydrothermalism in the Mediterranean Sea, *Progress*
496 *in Oceanography*, 44, 333–367, doi:10.1016/S0079-6611(99)00032-4,
497 <http://linkinghub.elsevier.com/retrieve/pii/S0079661199000324>, 1999.
- 498 Dutay, J.-C., Bullister, J., Doney, S., Orr, J., Najjar, R., Caldeira, K., Campin, J.-M., Drange, H.,
499 Follows, M., Gao, Y., Gruber, N., Hecht, M., Ishida, A., Joos, F., Lindsay, K., Madec, G.,
500 Maier-Reimer, E., Marshall, J., Matear, R., Monfray, P., Mouchet, A., Plattner, G.-K.,
501 Sarmiento, J., Schlitzer, R., Slater, R., Totterdell, I., Weirig, M.-F., Yamanaka, Y., and
502 Yool, A.: Evaluation of ocean model ventilation with CFC-11: comparison of 13 global
503 ocean models, *Ocean Modelling*, 4, 89–120, doi:10.1016/S1463-5003(01)00013-0,
504 [http://dx.doi.org/10.1016/S1463-5003\(01\)00013-](http://dx.doi.org/10.1016/S1463-5003(01)00013-0)
505 [0http://linkinghub.elsevier.com/retrieve/pii/S1463500301000130](http://linkinghub.elsevier.com/retrieve/pii/S1463500301000130), 2002.
- 506 Dutay, J.-C., Jean-Baptiste, P., Campin, J.-M., Ishida, A., Maier-Reimer, E., Matear, R.,
507 Mouchet, A., Totterdell, I., Yamanaka, Y., Rodgers, K., Madec, G., and Orr, J.:
508 Evaluation of OCMIP-2 ocean models’ deep circulation with mantle helium-3, *Journal of*
509 *Marine Systems*, 48, 15–36, doi:10.1016/j.jmarsys.2003.05.010, [https://hal.archives-](https://hal.archives-ouvertes.fr/hal-00154585)
510 [ouvertes.fr/hal-00154585](https://hal.archives-ouvertes.fr/hal-00154585), 2004.
- 511 Dutay, J. C., Emile-Geay, J., Iudicone, D., Jean-Baptiste, P., Madec, G., and Carouge, C.:
512 Helium isotopic constraints on simulated ocean circulations: Implications for abyssal
513 theories, *Environmental Fluid Mechanics*, 10, 257–273, doi:10.1007/s10652-009-9159-y,
514 2010.
- 515 Drobinski P., A. Anav, C. Lebeaupin Brossier, G. Sanson, M Stéfanon, S. Bastin, M Baklouti, K
516 Béranger, J Beuvier, R Bourdallé-Badie, L. Coquart, F D’andrea, N deNoblet, F Diaz, J-C
517 Dutay, C Ethé, M-A Foujols, D Khvorostiyannov, G Madec, E Maisonnave, M Mancip, S
518 Masson, L Menu, J Palmieri, J Polcher, S Turquety, S Valcke, N Viovy.: Model of
519 Regional Coupled Earthsystem (MORCE): application to process and climate studies in

520 [vulnerable regions](#), *Environmental Modelling and Software*, 35, 1-18, 2012

521 Elderfield, H. and Schultz, A.: Mid-Ocean Ridge Hydrothermal Fluxes and the Chemical
522 Composition of the Ocean, *Annual Review of Earth and Planetary Sciences*, 24, 191–224,
523 doi:10.1146/annurev.earth.24.1.191,
524 <http://www.annualreviews.org/doi/pdf/10.1146/annurev.earth.24.1.191>, 1996.

525 [England, M. H.: The age of water and ventilation timescales in a global ocean model](#). *J. Phys.*
526 *Oceanogr.*,25,2756–2777, 1995

527 Farley, K. A., Maier-Reimer, E., Schlosser, P., and Broecker, W. S.: Constraints on mantle ³He
528 fluxes and deep-sea circulation from an oceanic general circulation model, *Journal of*
529 *Geophysical Research*, 100, 3829, doi:10.1029/94JB02913,
530 <http://doi.wiley.com/10.1029/94JB02913>, 1995.

531 Ferry, N., Parent, L., Garric, G., Barnier, B., and Jourdain, N. C.: Mercator Global Eddy
532 Permitting Ocean Reanalysis GLORYS1V1: Description and Results, *Mercator Ocean*
533 *Quarterly Newsletter*, 36, 15–28, 2010.

534 Fiebig, J., Chiodini, G., Caliro, S., Rizzo, A., Spangenberg, J., and Hunziker, J. C.: Chemical
535 and isotopic equilibrium between CO₂ and CH₄ in fumarolic gas discharges: Generation of
536 CH₄ in arc magmatic hydrothermal systems, *Geochimica et Cosmochimica Acta*, 68, 2321–
537 2334, doi:10.1016/j.gca.2003.10.035,
538 <http://www.sciencedirect.com/science/article/pii/S0016703703008330>, 2004.

539 Fourré, E., Allard, P., Jean-Baptiste, P., Cellura, D., and Parello, F.: H³e/H⁴e Ratio in Olivines
540 from Linosa, Ustica, and Pantelleria Islands (Southern Italy), *Journal of Geological*
541 *Research*, 2012, 1–8, doi:10.1155/2012/723839, 2012.

542 GEOTRACE: GEOTRACES - An international study of the global marine biogeochemical
543 cycles of trace elements and their isotopes, *Chemie der Erde - Geochemistry*, 67, 85–131,
544 doi:10.1016/j.chemer.2007.02.001, 2007.

545 Goodman PJ. The Role of North Atlantic Deep Water Formation in an OGCM's Ventilation and
546 Thermohaline Circulation. *J. Phys. Oceanogr.* 1998;28(9):1759–1785. Available at:
547 [http://journals.ametsoc.org/doi/abs/10.1175/15200485\(1998\)028<1759:TRONAD>2.0.CO;](http://journals.ametsoc.org/doi/abs/10.1175/15200485(1998)028<1759:TRONAD>2.0.CO;2)
548 2, 1998.

549 Graham, D. W.: Noble Gas Isotope Geochemistry of Mid-Ocean Ridge and Ocean Island
550 Basalts: Characterization of Mantle Source Reservoirs, *Reviews in Mineralogy and*
551 *Geochemistry*, 47, 247–317, doi:10.2138/rmg.2002.47.8,
552 <http://rimg.geoscienceworld.org/cgi/doi/10.2138/rmg.2002.47.8>, 2002.

553 Herrmann, M., Sevault, F., Beuvier, J., and Somot, S.: What induced the exceptional 2005
554 convection event in the northwestern Mediterranean basin? Answers from a modeling

555 study, *Journal of Geophysical Research*, 115, C12 051, doi:10.1029/2010JC006162,
556 <http://doi.wiley.com/10.1029/2010JC006162>, 2010.

557 Herrmann, M. J. and Somot, S.: Relevance of ERA40 dynamical downscaling for modeling
558 deep convection in the Mediterranean Sea, *Geophysical Research Letters*, 35, L04 607,
559 doi:10.1029/2007GL032442, <http://doi.wiley.com/10.1029/2007GL032442>, 2008.

560 Hilton, D. R., Fischer, T. P., and Marty, B.: Noble Gases and Volatile Recycling at Subduction
561 Zones, *Reviews in Mineralogy and Geochemistry*, 47, 319–370,
562 doi:10.2138/rmg.2002.47.9, <http://rimg.geoscienceworld.org/content/47/1/319>, 2002.

563 Jähne, B., Heinz, G., and Dietrich, W.: Measurement of the diffusion coefficients of sparingly
564 soluble gases in water, *Journal of Geophysical Research*, 92, 10 767,
565 doi:10.1029/JC092iC10p10767, <http://doi.wiley.com/10.1029/JC092iC10p10767>, 1987a.

566 Jähne, B., Münnich, K. O., Bössinger, R., Dutzi, A., Huber, W., and Libner, P.: On the
567 parameters influencing air-water gas exchange, *Journal of Geophysical Research*, 92, 1937,
568 doi:10.1029/JC092iC02p01937, <http://doi.wiley.com/10.1029/JC092iC02p01937>, 1987b.

569 Jamous, D., Mémery, L., Andrié, C., Jean-Baptiste, P., and Merlivat, L.: The distribution of
570 helium 3 in the deep western and southern Indian Ocean, *Journal of Geophysical Research*,
571 97, 2243, doi:10.1029/91JC02062, <http://doi.wiley.com/10.1029/91JC02062>, 1992.

572 Jean-Baptiste, P., Charlou, J., Stievenard, M., Donval, J., Bougault, H., and Mevel, C.: Helium
573 and methane measurements in hydrothermal fluids from the mid-Atlantic ridge: The Snake
574 Pit site at 23°N, *Earth and Planetary Science Letters*, 106, 17–28, doi:10.1016/0012-
575 821X(91)90060-U, <http://www.sciencedirect.com/science/article/pii/0012821X9190060U>,
576 1991a.

577 Jean-Baptiste, P., Charlou, J. L., Stievenard, M., Donval, J., Bougault, H., and Mevel, C.:
578 Helium and methane measurements in hydrothermal fluids from the Mid Atlantic Ridge:
579 the SNAKE PIT site at 23°N, *Earth Planet. Sci. Lett.*, 106, 17–28, 1991b.

580 Jean-Baptiste, P., Mantsi, F., Memery, L., and Jamous, D.: Helium-3 and CFC in the Southern
581 Ocean: tracers of water masses, *Marine Chemistry*, 35, 137–150, 1992.

582 Jean-Baptiste, P., Dapoigny, A., Stievenard, M., Charlou, J. L., Fouquet, Y., Donval, J. P., and
583 Auzende, J. M.: Helium and oxygen isotope analyses of hydrothermal fluids from the East
584 Pacific Rise between 17°S and 19°S, *Geo-Marine Letters*, 17, 213–219,
585 doi:10.1007/s003670050029, <http://link.springer.com/10.1007/s003670050029>, 1997.

586 Jean-Baptiste, P., Fourré, E., Metz, N., Ternon, J., and Poisson, A.: Red Sea deep water
587 circulation and ventilation rate deduced from the 3He and 14C tracer fields, *Journal of*
588 *Marine Systems*, 48, 37–50, doi:10.1016/j.jmarsys.2003.07.001,
589 <http://adsabs.harvard.edu/abs/2004JMS...48...37J><http://linkinghub.elsevier.com/retrieve/pii>

590 /S0924796304000053, 2004.

591 Jenkins, D. J., Wolever, T. M., Leeds, A. R., Gassull, M. A., Haisman, P., Dilawari, J., Goff, D.
592 V., Metz, G. L., and Alberti, K. G.: Dietary fibres, fibre analogues, and glucose tolerance:
593 importance of viscosity., *Tech. Rep.* 6124, doi:10.1136/bmj.1.6124.1392,
594 [http://www.pubmedcentral.nih.gov/articlerender.fcgi?artid=1604761&tool=pmcentrez&ren](http://www.pubmedcentral.nih.gov/articlerender.fcgi?artid=1604761&tool=pmcentrez&rendertype=abstract)
595 [dertype=abstract](http://www.pubmedcentral.nih.gov/articlerender.fcgi?artid=1604761&tool=pmcentrez&rendertype=abstract), 1978.

596 Jenkins, W. and Clarke, W.: The distribution of ³He in the western Atlantic ocean, *Deep Sea*
597 *Research and Oceanographic Abstracts*, 23, 481–494, doi:10.1016/0011-7471(76)90860-
598 3,<http://www.sciencedirect.com/science/article/pii/0011747176908603>[http://linkinghub.else](http://linkinghub.elsevier.com/retrieve/pii/0011747176908603)
599 [vier.com/retrieve/pii/0011747176908603](http://linkinghub.elsevier.com/retrieve/pii/0011747176908603), 1976.

600 Jenkins, W. J.: Tritium-helium dating in the sargasso sea: a measurement of oxygen utilization
601 rates., *Science (New York, N.Y.)*, 196, 291–2 doi:10.1126/science.196.4287.291,
602 <http://www.ncbi.nlm.nih.gov/pubmed/17756096>, 1977.

603 Jenkins, W. J.: The use of Anthropogenic Tritium and He-3 to Study Sub-Tropical Gyre
604 Ventilation and Circulation, *Philosophical Transactions of the Royal Society of London*
605 *Series A-Mathematical Physical and Engineering Sciences*, 325, 43 – 61, 1988.

606 Kato, Y., Fujinaga, K., Nakamura, K., Takaya, Y., Kitamura, K., Ohta, J., Toda, R., Nakashima,
607 T., and Iwamori, H.: Deep-sea mud in the Pacific Ocean as a potential resource for rare-
608 earth elements, *Nature Geoscience*, 4, 535–539, doi:10.1038/ngeo1185,
609 <http://dx.doi.org/10.1038/ngeo1185>, 2011.

610 Kipfer, R., Aeschbach-Hertig, W., Peeters, F., and Stute, M.: Noble Gases in Lakes and
611 Groundwaters, *Reviews in Mineralogy and Geochemistry*, 47, 615–700,
612 doi:10.2138/rmg.2002.47.14, <http://rimg.geoscienceworld.org/content/47/1/615.extract>,
613 2002.

614 Lebeaupin Brossier, C., Béranger, K., Deltel, C., and Drobinski, P.: The Mediterranean response
615 to different space–time resolution atmospheric forcings using perpetual mode sensitivity
616 simulations, *Ocean Modelling*, 36, 1–25, doi:10.1016/j.ocemod.2010.10.008,
617 <http://www.sciencedirect.com/science/article/pii/S1463500310001642>, 2011.

618 Locarnini, R. A., Mishonov, A. V., Antonov, J. I., Boyer, T. P., and Garcia, H. E.: *World Ocean*
619 *Atlas 2005, Volume 1: Temperature*, S. Levitus, Ed, NOAA Atlas NESDIS 61, U.S.
620 Government Printing Office, Washington, D.C. 182 pp, 2006.

621 Ludwig, W., Dumont, E., Meybeck, M., and Heussner, S.: River discharges of water and
622 nutrients to the Mediterranean and Black Sea: Major drivers for ecosystem changes during
623 past and future decades?, *Progress in Oceanography*, 80, 199–217,
624 doi:10.1016/j.pocean.2009.02.001,

625 <http://www.sciencedirect.com/science/article/pii/S0079661109000020>, 2009.

626 Lupton, J.: Hydrothermal helium plumes in the Pacific Ocean, *Journal of Geophysical Research*,
627 103, 15 853,doi:10.1029/98JC00146, <http://doi.wiley.com/10.1029/98JC00146>, 1998.

628 Lupton, J., de Ronde, C., Sprovieri, M., Baker, E. T., Bruno, P. P., Italiano, F., Walker, S.,
629 Faure, K., Ley530 bourne, M., Britten, K., and Greene, R.: Active hydrothermal discharge
630 on the submarine Aeolian Arc,
631 *Journal of Geophysical Research*, 116, B02 102, doi:10.1029/2010JB007738,
632 <http://doi.wiley.com/10.1029/2010JB007738>, 2011.

633 Lupton, J. E.: Helium-3 in the Guaymas Basin: Evidence for injection of mantle volatiles in the
634 Gulf of California,*Journal of Geophysical Research*, 84, 7446,
635 doi:10.1029/JB084iB13p07446, <http://doi.wiley.com/10.1029/JB084iB13p07446>, 1979.

636 Lupton, J. E.: A Far-Field Hydrothermal Plume from Loihi Seamount, *Science*, 272, 976–
637 979,doi:10.1126/science.272.5264.976,<http://www.ncbi.nlm.nih.gov/pubmed/8662580><http://www.sciencemag.org/cgi/doi/10.1126/science.272.5264.976>, 1996.

638

639 Lupton, J. E., Weiss, R. F., and Craig, H.: Mantle helium in the Red Sea brines, *Nature*, 266,
640 244–246, doi:10.1038/266244a0,
641 [http://apps.webofknowledge.com/full_record.do?mode=FullRecord&excludeEventConfig=](http://apps.webofknowledge.com/full_record.do?mode=FullRecord&excludeEventConfig=ExcludeIfFromFullRecPage&UT=WOS:A1977CY57200028&qid=10&log_event=yes&viewType=fullRecord&SID=X132NgYZaFieda7ZJya&SID=X132NgYZaFieda7ZJya&product=WOS&product=WOS&SrcApp=Wile)
642 [ExcludeIfFromFullRecPage&UT=WOS:A1977CY57200028&qid=10&log_event=yes&vie](http://apps.webofknowledge.com/full_record.do?mode=FullRecord&excludeEventConfig=ExcludeIfFromFullRecPage&UT=WOS:A1977CY57200028&qid=10&log_event=yes&viewType=fullRecord&SID=X132NgYZaFieda7ZJya&SID=X132NgYZaFieda7ZJya&product=WOS&product=WOS&SrcApp=Wile)
643 [wType=fullRecord&SID=X132NgYZaFieda7ZJya&SID=X132NgYZaFieda7ZJya&produ](http://apps.webofknowledge.com/full_record.do?mode=FullRecord&excludeEventConfig=ExcludeIfFromFullRecPage&UT=WOS:A1977CY57200028&qid=10&log_event=yes&viewType=fullRecord&SID=X132NgYZaFieda7ZJya&SID=X132NgYZaFieda7ZJya&product=WOS&product=WOS&SrcApp=Wile)
644 [ct=WOS&product=WOS&SrcApp=Wile](http://apps.webofknowledge.com/full_record.do?mode=FullRecord&excludeEventConfig=ExcludeIfFromFullRecPage&UT=WOS:A1977CY57200028&qid=10&log_event=yes&viewType=fullRecord&SID=X132NgYZaFieda7ZJya&SID=X132NgYZaFieda7ZJya&product=WOS&product=WOS&SrcApp=Wile), 1977a.

645 Lupton, J. E., Weiss, R. F., and Craig, H.: Mantle helium in hydrothermal plumes in the
646 Galapagos Rift, *Nature*, 267, 603–604, doi:10.1038/267603a0,
647 [http://apps.webofknowledge.com/full_record.do?mode=FullRecord&excludeEventConfig=](http://apps.webofknowledge.com/full_record.do?mode=FullRecord&excludeEventConfig=ExcludeIfFromFullRecPage&UT=WOS:A1977DJ69100024&qid=1&log_event=yes&viewType=fullRecord&SID=X132NgYZaFieda7ZJya&SID=X132NgYZaFieda7ZJya&product=WOS&product=WOS&SrcApp=Wiley)
648 [ExcludeIfFromFullRecPage&UT=WOS:A1977DJ69100024&qid=1&log_event=yes&view](http://apps.webofknowledge.com/full_record.do?mode=FullRecord&excludeEventConfig=ExcludeIfFromFullRecPage&UT=WOS:A1977DJ69100024&qid=1&log_event=yes&viewType=fullRecord&SID=X132NgYZaFieda7ZJya&SID=X132NgYZaFieda7ZJya&product=WOS&product=WOS&SrcApp=Wiley)
649 [Type=fullRecord&SID=X132NgYZaFieda7ZJya&SID=X132NgYZaFieda7ZJya&product](http://apps.webofknowledge.com/full_record.do?mode=FullRecord&excludeEventConfig=ExcludeIfFromFullRecPage&UT=WOS:A1977DJ69100024&qid=1&log_event=yes&viewType=fullRecord&SID=X132NgYZaFieda7ZJya&SID=X132NgYZaFieda7ZJya&product=WOS&product=WOS&SrcApp=Wiley)
650 [=WOS&product=WOS&SrcApp=Wiley](http://apps.webofknowledge.com/full_record.do?mode=FullRecord&excludeEventConfig=ExcludeIfFromFullRecPage&UT=WOS:A1977DJ69100024&qid=1&log_event=yes&viewType=fullRecord&SID=X132NgYZaFieda7ZJya&SID=X132NgYZaFieda7ZJya&product=WOS&product=WOS&SrcApp=Wiley), 1977b.

651 Madec, G. and NEMO-Team.: Note du Pôle de modélisation, Institut Pierre-Simon Laplace
652 (IPSL), France, NEMO ocean engine, 27, doi:ISSN N1288-1619, 2008.

653 Martelli, M., Caracausi, A., Paonita, A., and Rizzo, A.: Geochemical variations of air-free crater
654 fumaroles at MtEtna: New inferences for forecasting shallow volcanic activity,
655 *Geophysical Research Letters*, 35, L21 302,doi:10.1029/2008GL035118,
656 <http://doi.wiley.com/10.1029/2008GL035118>, 2008.

657 MEDAR-MedAtlas-group: Medar-Medatlas Protocol (Version 3) Part I: Exchange Format and
658 Quality Checks for Observed Profiles, P. Rap. Int. IFREMER/TMSI/IDM/SIS002-006, 50,
659 2002.

- 660 Palmiéri, J., Orr, J. C., Dutay, J.-C., Béranger, K., Schneider, A., Beuvier, J., and Somot, S.:
661 Simulated anthropogenic CO₂ storage and acidification of the Mediterranean
662 Sea, *Biogeosciences*, 12, 781–802, doi:10.5194/bg-12-781-2015,
663 <http://www.biogeosciences.net/12/781/2015/bg-12-781-2015.html>, 2015.
- 664 Parello, F., Allard, P., D’Alessandro, W., Federico, C., Jean-Baptiste, P., and Catani, O.: Isotope
665 geochemistry of Pantelleria volcanic fluids, Sicily Channel rift: a mantle volatile end-
666 member for volcanism in southern
667 Europe, *Earth and Planetary Science Letters*, 180, 325–339, doi:10.1016/S0012-
668 821X(00)00183-7, <http://adsabs.harvard.edu/abs/2000E%26PSL.180..325P>, 2000.
- 669 Rhein, M., U. Send, B. Klein and G. Krahnemann, *Interbasin deep water exchange in the western*
670 *Mediterranean. J. Geophys. Res.*, 104(C10), 23495-23508, 1999.
- 671 Rixen, M., Beckers, J. M., Levitus, S., Antonov, J., Boyer, T., Maillard, C., Fichaut, M.,
672 Balopoulos, E., Iona, S., Dooley, H., Garcia, M. J., Manca, B., Giorgetti, A., Manzella, G.,
673 Mikhailov, N., Pinardi, N., and Zavatarelli, M.: The Western Mediterranean Deep Water: A
674 proxy for climate change, *Geophysical Research Letters*, 32, 1–4,
675 doi:10.1029/2005GL022702, <http://doi.wiley.com/10.1029/2005GL022702>, 2005.
- 676 Roether, W. and Lupton, J. E.: Tracers confirm downward mixing of Tyrrhenian Sea upper
677 waters associated with the Eastern Mediterranean Transient, *Ocean Science*, 7, 91–99,
678 doi:10.5194/os-7-91-2011, <http://www.ocean-sci.net/7/91/2011/os-7-91-2011.html>, 2011.
- 679 Roether, W., Roussenov, V. M., and Well, R.: A tracer study of the thermohaline circulation of
680 the eastern Mediterranean, *Ocean Processes in Climate Dynamics: Global and*
681 *Mediterranean Examples*, pp. 371–394, 1994.
- 682 Roether, W., Well, R., Putzka, A., and Rùth, C.: Component separation of oceanic helium,
683 doi:10.1029/98JC02234, <http://doi.wiley.com/10.1029/98JC02234>, 1998.
- 684 Roether, W., Well, R., Putzka, A., Ruth, C. Correction to “Component separation of oceanic
685 helium” by Wolfgang Roether, Roland Well, Alfred Putzka and Christina Ruth. *J.*
686 *Geophys. Res.* 106, 4679, 2001.
- 687 Roether, W., Jean-Baptiste, P., Fourné, E., and Sùltenfuß, J.: The transient distributions of
688 nuclear weapongenerated tritium and its decay product ³He in the
689 Mediterranean Sea, 1952–2011, and their oceanographic potential, *Ocean Science*, 9, 837–
690 854, doi:10.5194/os-9-837-2013, <http://www.ocean-sci.net/9/837/2013/os-9-837->
691 [2013.html](http://www.ocean-sci.net/9/837/2013/os-9-837-2013.html), 2013.
- 692 Roether, W., Klein, B., and Hainbucher, D.: *The Eastern Mediterranean Transient : Evidence for*
693 *Similar, The Mediterranean Sea: Temporal Variability and Spatial Patterns, Geophysical*
694 *Monograph 202. First Edition ,American Geophysical Union, 12, 75–83, 2014.*

- 695 R uth, C., Well, R., and Roether, W.: Primordial in South Atlantic deep waters from sources on
696 the Mid-Atlantic Ridge, *Deep Sea Research Part I: Oceanographic Research Papers*, 47,
697 1059–1075, doi:10.1016/S0967-0637(99)00077-1,
698 <http://www.sciencedirect.com/science/article/pii/S0967063799000771><http://linkinghub.elsevier.com/retrieve/pii/S0967063799000771>, 2000.
- 700 Sano, T., Hataya, T., Terai, Y., and Shikata, E.: Hop stunt viroid strains from dapple fruit
701 disease of plum and peach in Japan., *The Journal of general virology*, 70 (Pt 6), 1311–9,
702 <http://www.ncbi.nlm.nih.gov/pubmed/5852732717>, 1989.
- 703 Sano, Y. and Wakita, H.: Geographical distribution of $^3\text{He}/^4\text{He}$ ratios in Japan: Implications
704 for arc tectonics and incipient magmatism, *Journal of Geophysical Research*, 90, 8729,
705 doi:10.1029/JB090iB10p08729, <http://doi.wiley.com/10.1029/JB090iB10p08729>, 1985.
- 706 Sano, Y., Wakita, H., Ohsumi, T., and Kusakabe, M.: Helium isotope evidence for magmatic
707 gases in Lake Nyos, Cameroon, *Geophysical Research Letters*, 14, 1039–1041,
708 doi:10.1029/GL014i010p01039, <http://doi.wiley.com/10.1029/GL014i010p01039>, 1987.
- 709 Schlosser, P. and Winckler, G.: Noble Gases in Ocean Waters and Sediments, *Reviews in*
710 *Mineralogy and Geochemistry*, 47, 701–730, doi:10.2138/rmg.2002.47.15,
711 <http://rimg.geoscienceworld.org/content/47/1/701.extract><http://rimg.geoscienceworld.org/cgi/doi/10.2138/rmg.2002.47.15>, 2002.
- 713 Schlosser, P., Bullister, J. L., and Bayer, R.: Studies of deep water formation and circulation in
714 the Weddell Sea using natural and anthropogenic tracers, *Marine Chemistry*, 35, 97–122,
715 doi:10.1016/S0304-4203(09)90011-1,
716 <http://www.sciencedirect.com/science/article/pii/S0304420309900111>, 1991.
- 717 Shimizu, A., Sumino, H., Nagao, K., Notsu, K., and Mitropoulos, P.: Variation in noble gas
718 isotopic composition of gas samples from the Aegean arc, Greece, *Journal of Volcanology*
719 *and Geothermal Research*, 140, 321–339, doi:10.1016/j.jvolgeores.2004.08.016,
720 <http://www.sciencedirect.com/science/article/pii/S0377027304003130>, 2005.
- 721 Soto-Navarro, J., Somot, S., Sevault, F., Beuvier, J., B ranger, K., Criado-Aldeanueva, F., and
722 Garc a-Lafuente, J.: Evaluation of regional ocean circulation models for the Mediterranean
723 Sea at the Strait of Gibraltar : volume transport and thermohaline properties of the outflow,
724 *Climate Dynamics*, doi:10.1007/s00382-014-2179-4,
725 <http://link.springer.com/10.1007/s00382-014-2179-4>, 2014.
- 726 Srinivasan, A., Top, Z., Schlosser, P., Hohmann, R., Iskandarani, M., Olson, D. B., Lupton, J.
727 E., and Jenkins, W. J.: Mantle ^3He distribution and deep circulation in the Indian Ocean,
728 <https://darchive.mblwhoilibrary.org/handle/1912/3711>, 2004.
- 729 Tagliabue, A., Bopp, L., Dutay, J.-C., Bowie, A. R., Chever, F., Jean-Baptiste, P., Bucciarelli,

- 730 E., Lannuzel, D., Remenyi, T., Sarthou, G., Aumont, O., Gehlen, M., and Jeandel, C.:
731 Hydrothermal contribution to the oceanic dissolved iron inventory, *Nature Geoscience*, 3,
732 252–256, doi:10.1038/ngeo818, <http://dx.doi.org/10.1038/ngeo818>, 2010.
- 733 Taylor, S. and McLennan, S.: *The Continental Crust; Its composition and evolution; an*
734 *examination of the geochemical record preserved in sedimentary rocks*, Blackwell, Oxford,
735 312, 1985.
- 736 Tedesco, D. and Scarsi, P.: Intensive gas sampling of noble gases and carbon at Vulcano Island
737 (southern Italy), *Journal of Geophysical Research*, 104, 10 499,
738 doi:10.1029/1998JB900066, <http://doi.wiley.com/10.1029/1998JB900066>, 1999.
- 739 Tedesco, D., Miele, G., Sano, Y., and Toutain, J. P.: Helium isotopic ratio in Vulcano island
740 fumaroles: temporal variations in shallow level mixing and deep magmatic supply, *Journal*
741 *of Volcanology and Geothermal Research*, 64, 117–128, doi:10.1016/0377-
742 0273(94)00045-I, <http://www.sciencedirect.com/science/article/pii/037702739400045I>,
743 1995.
- 744 Top, Z. and Clarke, W. B.: Helium, neon, and tritium in the Black Sea, *Journal of Marine*
745 *Research*, 41, 1–17, doi:10.1357/002224083788223045,
746 <http://www.ingentaconnect.com/content/jmr/jmr/1983/00000041/00000001/art00001>
747 <http://openurl.ingenta.com/content/xref?genre=article&issn=0022->
748 [2402&volume=41&issue=1&spage=1](http://openurl.ingenta.com/content/xref?genre=article&issn=0022-2402&volume=41&issue=1&spage=1), 1983.
- 749 Top, Z., Östlund, G., Pope, L., and Grall, C.: Helium isotopes, neon and tritium in the Black
750 Sea: A comparison with the 1975 observations, *Deep Sea Research Part A. Oceanographic*
751 *Research Papers*, 38, S747–S759, doi:10.1016/S0198-0149(10)80007-X,
752 <http://www.sciencedirect.com/science/article/pii/S019801491080007X>
753 <http://linkinghub.elsevier.com/retrieve/pii/S019801491080007X>, 1991.
- 754 Torgersen, T.: Terrestrial helium degassing fluxes and the atmospheric helium budget:
755 Implications with respect to the degassing processes of continental crust, *Chemical*
756 *Geology: Isotope Geoscience section*, 79, 1–14, doi:10.1016/0168-9622(89)90002-X,
757 <http://www.sciencedirect.com/science/article/pii/016896228990002X>, 1989.
- 758 Torgersen, T.: Continental degassing flux of 4 He and its variability, *Geochemistry, Geophysics,*
759 *Geosystems*, 11, n/a–n/a, doi:10.1029/2009GC002930,
760 <http://doi.wiley.com/10.1029/2009GC002930>, 2010.
- 761 Vörösmarty, C. J., Fekete, B. M., and Tucker, B. A.: *Global River Discharge Database (RivDIS*
762 *V1.0)*, International Hydrological Program, Global Hydrological Archive and Analysis
763 Systems, UNESCO, Paris, 1996.
- 764 Wanninkhof, R.: Relationship between wind speed and gas exchange over the ocean, *Journal of*

765 Geophysical Research, 97, 7373, doi:10.1029/92JC00188,
766 <http://doi.wiley.com/10.1029/92JC00188>, 1992.

767 Weiss, R. F.: Solubility of helium and neon in water and seawater, Journal of Chemical &
768 Engineering Data, 16, 235–241, doi:10.1021/je60049a019,
769 <http://pubs.acs.org/doi/abs/10.1021/je60049a019>, 1971.

770 Weiss, W. and Roether, W.: The rates of tritium input to the world oceans, Earth and Planetary
771 Science Letters, 49, 435–446, doi:10.1016/0012-821X(80)90084-9,
772 <http://www.sciencedirect.com/science/article/pii/0012821X80900849>, 1980.

773 Well, R., Lupton, J., and Roether, W.: Crustal helium in deep Pacific waters, Journal of
774 Geophysical Research, 106, 14 165, doi:10.1029/1999JC000279,
775 <http://doi.wiley.com/10.1029/1999JC000279>, 2001.

776 Winckler, G., Suess, E., Wallmann, K., de Lange, G. J., Westbrook, G. K., and Bayer, R.:
777 Excess helium and argon of radiogenic origin in Mediterranean brine basins, Earth and
778 Planetary Science Letters, 151, 225–231, doi:10.1016/S0012-821X(97)81850-X,
779 <http://www.sciencedirect.com/science/article/pii/S0012821X9781850X>, 1997.

780
781
782

783 **Table 1:** Release rates of mantle helium in the Mediterranean Sea used in the model (see §3.1.3).

Region	Prescribed ^3He Flux	$^3\text{He} / ^4\text{He}$	References
Tyrrhenian basin:			
Eolian Arc	0.8 (mol yr ⁻¹)	6 Ra	Sano et al. (1989); Tedesco et al. (1995); Tedesco and Scarsi (1999); Capasso et al. (2005); Capaccioni et al. (2007); Martelli et al. (2008); Fourré et al. (2012)
Marsili Seamount	0.4 (mol yr ⁻¹)		
Aegean basin:			
South Aegean Arc	1.5 (mol yr ⁻¹)	4 Ra	Fiebig et al. (2004); Shimizu et al. (2005); D’Alessandro et al. (1997)
Sicily Channel:			
Pantelleria Rift	0.8 (mol yr ⁻¹)	8 Ra	(Parello et al., 2000)

784
785
786

787
788
789

Table 2 : Release rate of crustal helium used in the model and comparison with crustal helium fluxes in various geological settings.

Region	^3He (mol m ⁻² yr ⁻¹)	^4He (mol m ⁻² yr ⁻¹)	References
Mediterranean Sea	1.32×10^{-14}	1.6×10^{-7}	This work
Continental Crust	4.7×10^{-14}	1.4×10^{-6}	(Torgersen, 1989)
Continental Crust	–	2.2×10^{-6}	(Torgersen, 2010)
Eastern Med	–	1.6×10^{-6}	(Roether et al., 1998)
Black Sea	5.8×10^{-13}	0.7×10^{-6}	(Top and Clarke, 1983)
Global Ocean Floor	$(1.5\text{--}4.6) \times 10^{-15}$	$(0.2\text{--}1.4) \times 10^{-7}$	(Torgersen, 1989)
Pacific Ocean	–	$(0.01\text{--}0.2) \times 10^{-7}$	(Sano et al., 1987)
Pacific Ocean	–	0.75×10^{-7}	(Well et al., 2001)

790
791
792
793
794
795
796
797
798
799
800
801
802

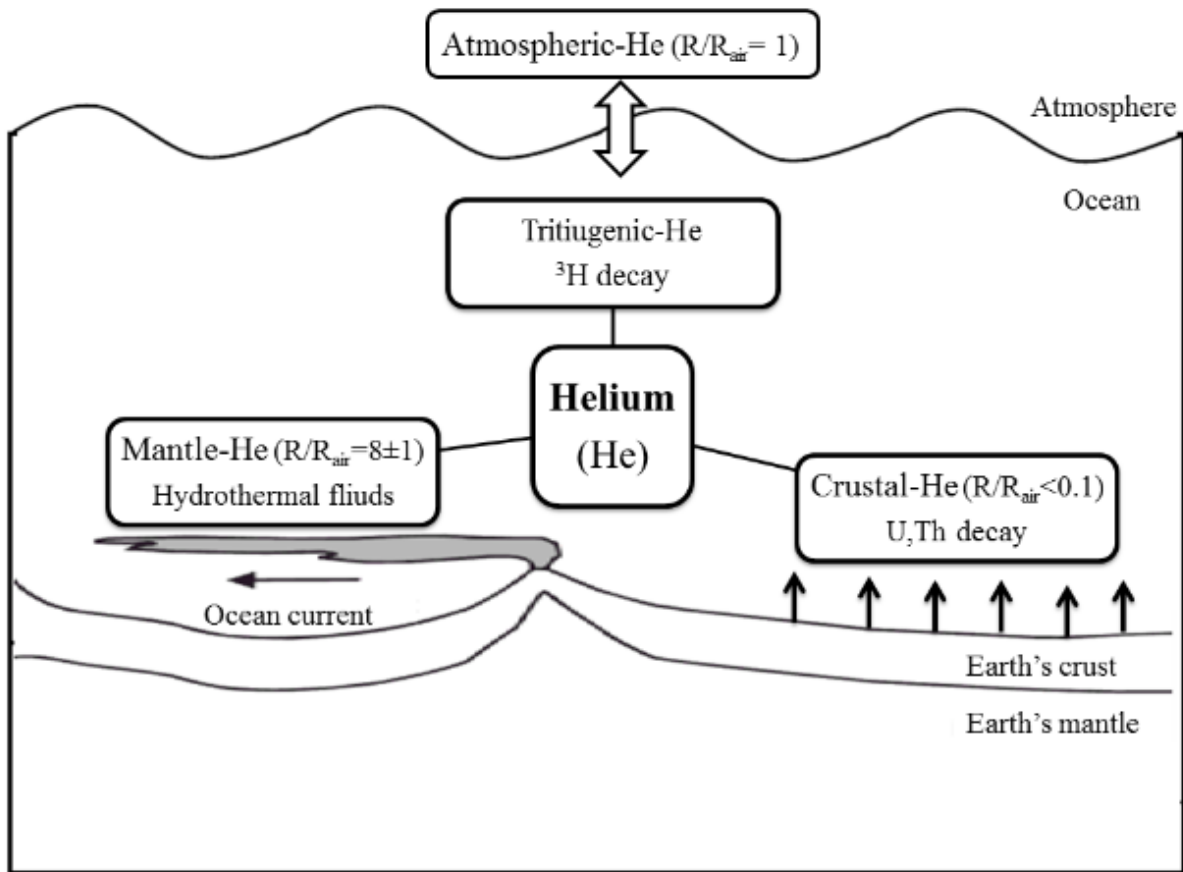
Table 3: Helium inventory (in mole) in the Mediterranean Sea.

	Helium-3	% (Terrigenic)	Helium-4	% (Terrigenic)
Mantle	5	0.8	6.04×10^5	0.3
Crust	18	2.9	2.18×10^8	99.3
Tritogenic (1987)	599	96.3	0	0
Atmospheric	9070		6.67×10^9	
Total	9692		6.89×10^9	

803
804

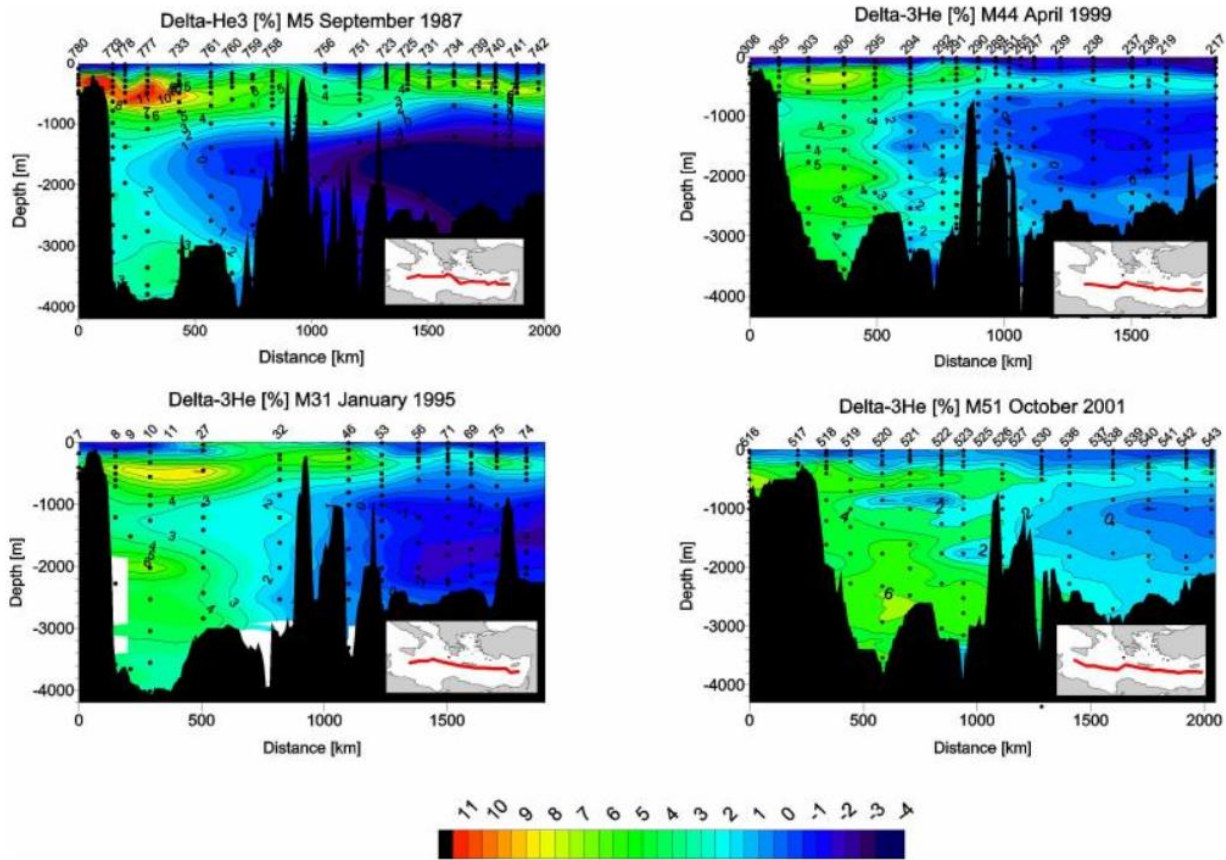
805

806

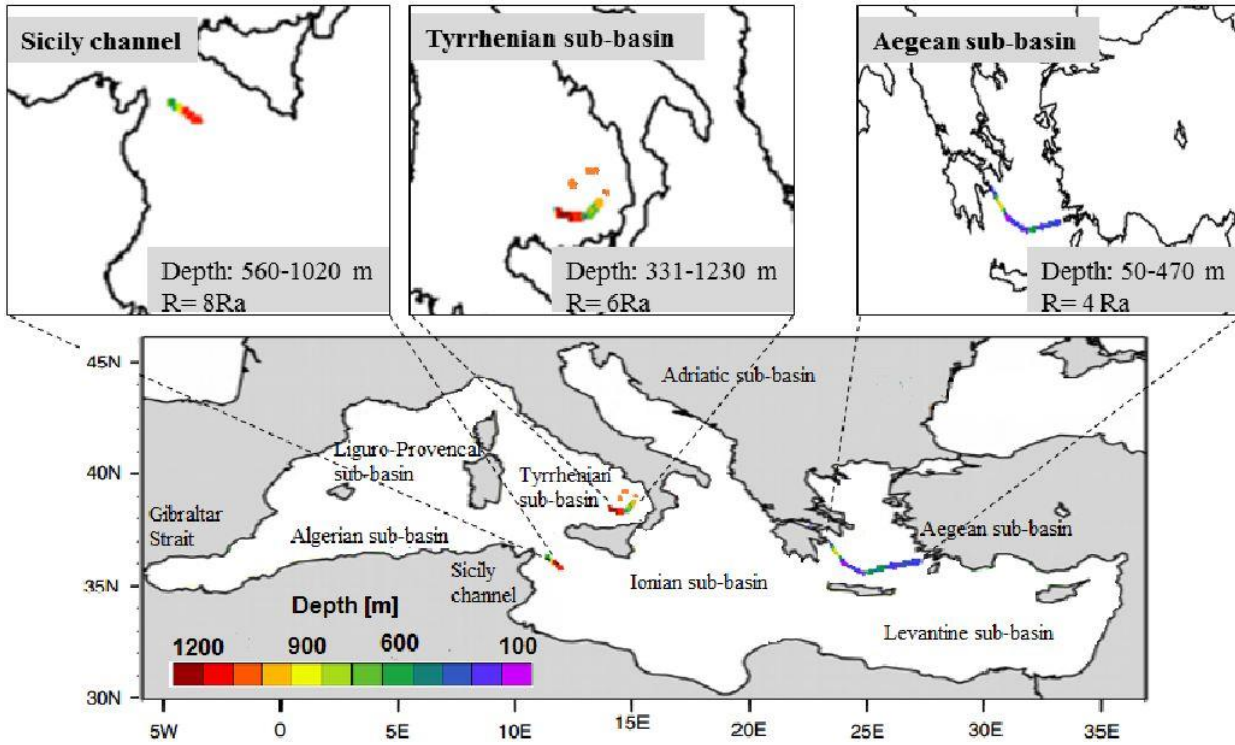


807

808 **Fig. 1.** Schematic of helium components in the ocean. Most of the crustal helium consists of
 809 ^4He , and most of the mantle helium consists of ^3He . Note that the tritiogenic component consists
 810 of ^3He only. Helium in solution at the ocean surface, is essentially in equilibrium with
 811 atmospheric He.



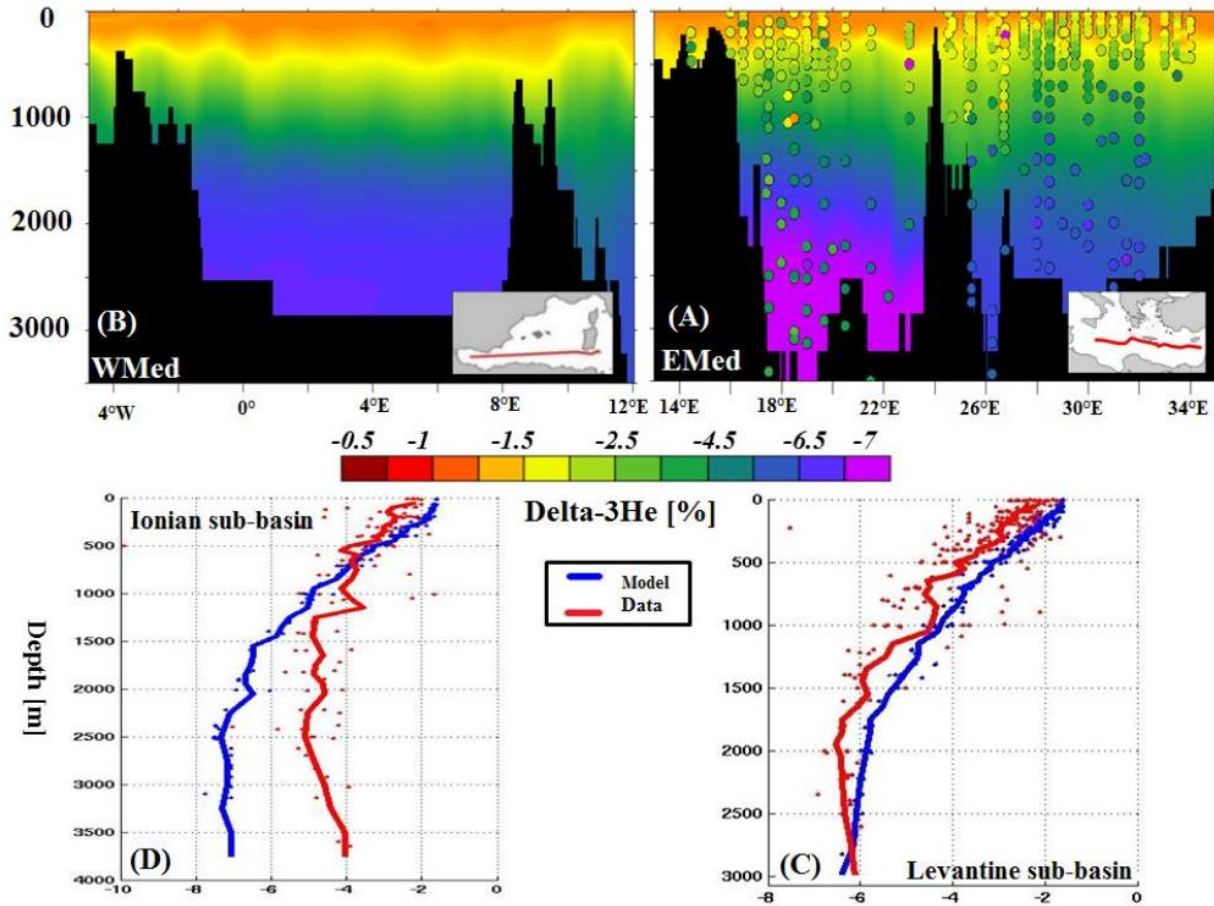
812
 813 **Fig. 2.** $\delta^3\text{He}$ sections of the Meteor cruises in 1987, 1995, 1999 and 2001. Numbers on top are
 814 station numbers, observations are indicated by dots, and the actual sections are shown in the
 815 inset maps. Isolines are by objective mapping (reproduced from Roether et al., 2013).



816
817

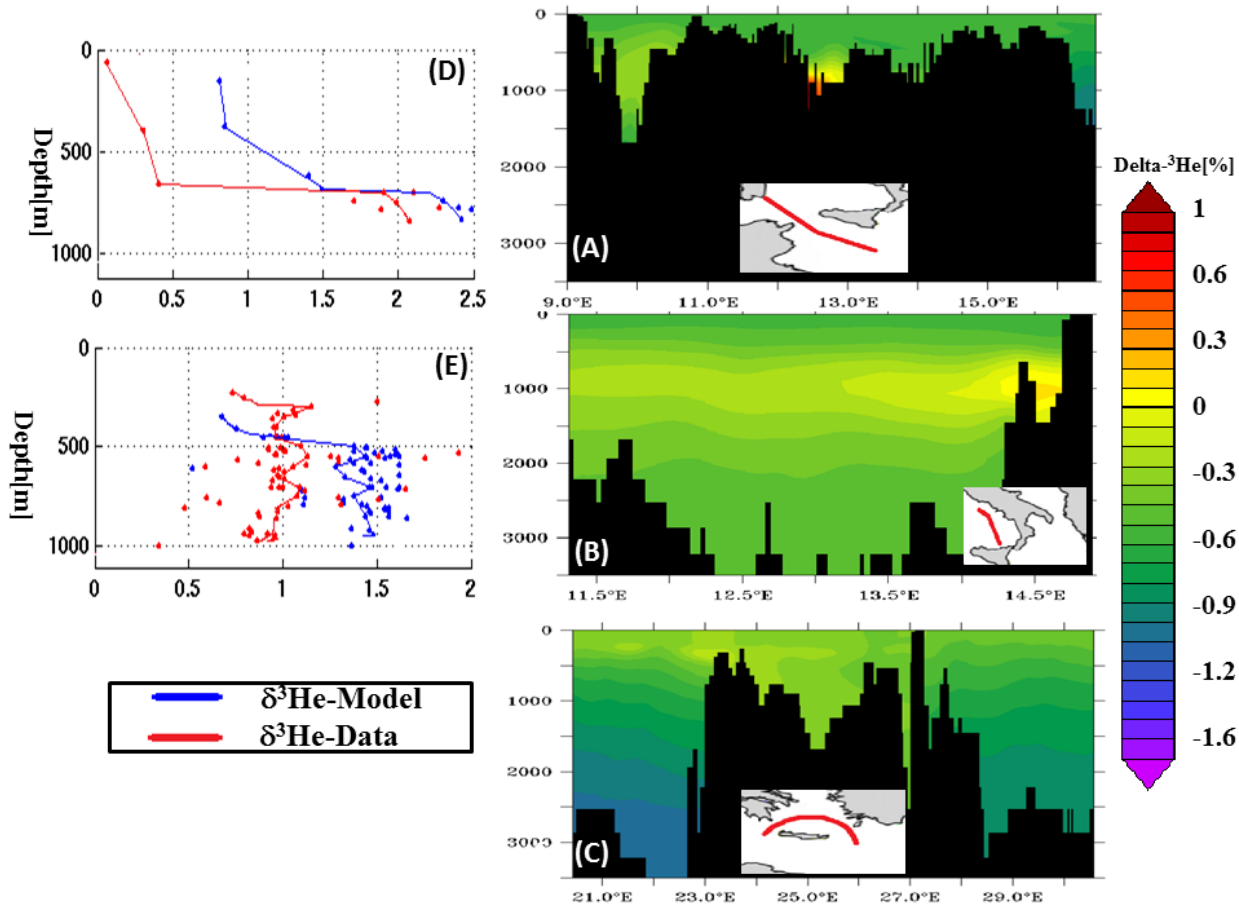
Fig. 3. Depth (in metres) and localization of mantle helium injection in the Mediterranean Sea.

818



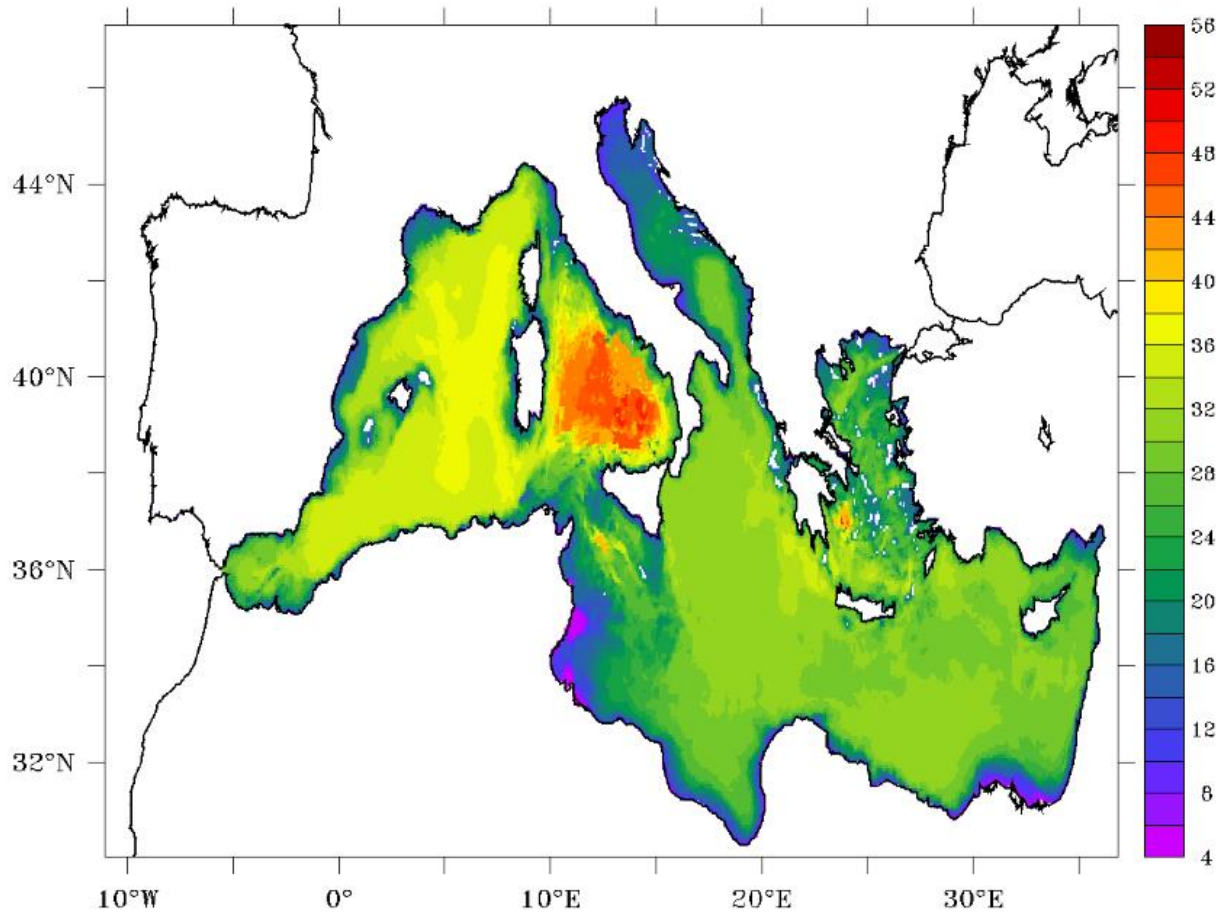
819

820 **Fig. 4.** Crustal+atmospheric $\delta^3\text{He}$ (in %) model-data comparison along the Meteor M5
 821 (September 1987) section: (a) Colour-filled contours indicate simulated $\delta^3\text{He}$ (%), whereas
 822 colour-filled dots represent the crustal+atmospheric $\delta^3\text{He}$ deduced from in situ observations
 823 using the component separation method of Roether et al., 1998 in the eastern basin (see §4 for
 824 details). (b) idem for the western basin (WMed). There are no quantitative data for comparison
 825 in the WMed (c) and (d) Comparison of average vertical profiles along the Meteor M5/9-1987
 826 section for the Levantine and the Ionian sub-basins respectively: model results are in blue; red
 827 indicates the in situ data.



828

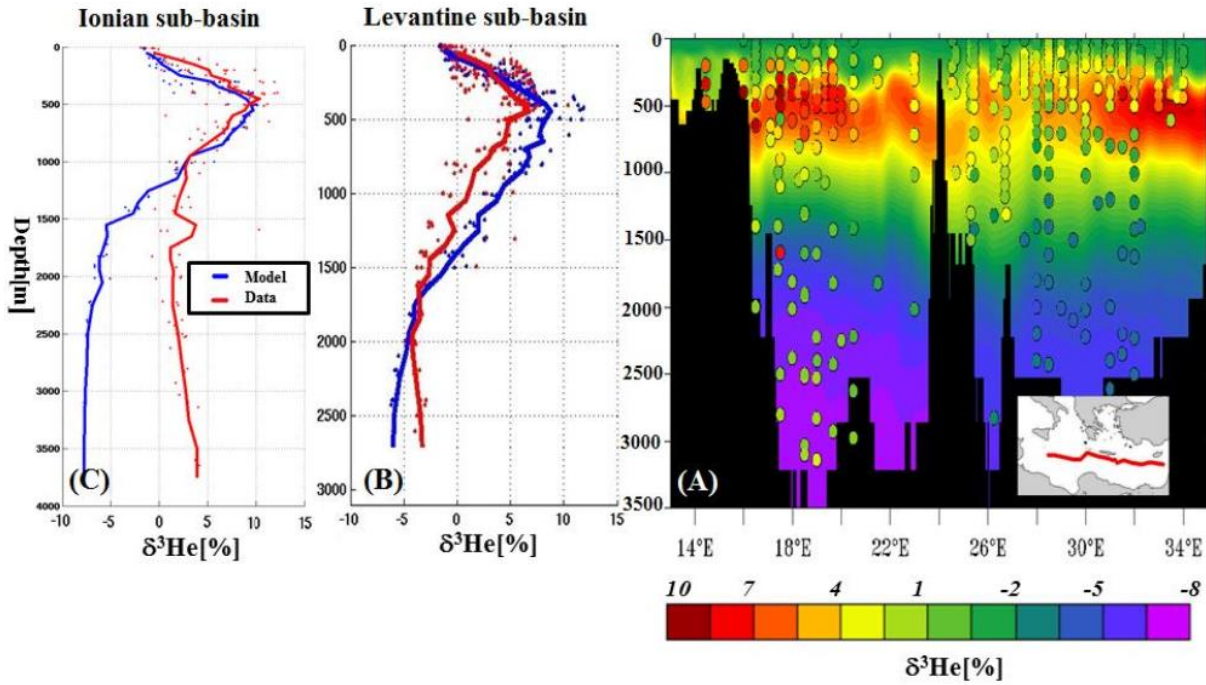
829 **Fig. 5.** Mantle+atmospheric $\delta^3\text{He}$ (%) model-data comparison in (a) the Sicily channel, (b)
 830 Tyrrhenian sub-basin, and (c) Aegean sub-basin. (d) Vertical profiles of $\delta^3\text{He}$ (above the
 831 atmospheric background of -1.6%) at 12°E in the Sicily channel: model results are in blue; red
 832 indicates in situ data (Fourré and Jean-Baptiste, unpublished results). (e) Same as (d) for the
 833 Tyrrhenian sub-basin. The data are from Lupton et al. (2011). The few stations located right
 834 above a plume in Lupton et al. (2011) have been discarded because they cannot be compared to
 835 model results which are averaged over the volume of the model cell ($\sim 20 \text{ km}^3$). There are no
 836 data for the Aegean basin.



837
838

Fig. 6. Horizontal distribution of $\delta^3\text{He}_{\text{mantle}}$ (vertically integrated) across the Mediterranean Sea.

839
840
841



842
 843 **Fig. 7.** Total $\delta^3\text{He}$ (sum of terrigenic, tritiogenic and atmospheric helium) model-data
 844 comparison along the Meteor M5 (September 1987) section. (a) Colour-filled contours indicate
 845 simulated $\delta^3\text{He}$ (%), whereas colour-filled dots represent in situ observations. (b) and (c)
 846 Comparison of average vertical profiles for the Levantine and the Ionian sub-basins
 847 respectively. Model results are in blue; red indicates in situ data.
 848

849
 850

851

